Open-Phase Fault-Tolerant Operation of the Three-Phase Dual Active Bridge Converter

Maxime Berger, *Student Member, IEEE*, Ilhan Kocar, *Senior Member, IEEE*, Handy Fortin-Blanchette, *Member, IEEE*, and Carl Lavertu, *Member, IEEE*

***Abstract*—The three-phase dual active bridge (3p-DAB) converter is widely considered in dc-grid applications. Because of the higher number of switches in the 3p-DAB, it can be argued that the reliability of the 3p-DAB is reduced when compared to other isolated-bidirectional dc–dc converter topologies. The previous work has shown that the 3p-DAB can be operated in a frozen leg fault-tolerant mode, i.e., with the two transistors of the same phase being opened by their gate driver internal protections. Because the free-wheeling diodes are left self-commutated, the analytical characterization of the converter for all voltage and loading conditions is not trivial. In this article, it is proposed to open the faulty phase such as it eliminates the interaction with the faulty-phase free-wheeling diodes. This allows the converter to fall in a characterizable operating mode for all voltage and loading conditions. The results further show that the open-phase operation provides advantages over the frozen leg operation in terms of current stress and power transfer capability. Experimental results on a small-scale closed-loop gallium nitride-based prototype as well as time-domain simulation results are provided to support the theoretical analyses.**

***Index Terms*—DC-DC power converters, fault tolerance, systems modeling.**

I. Introduction

POWER electronics interfaces play a key role in dc-grids [1], their primary functions being power flow control and voltage conversion between different grid voltage levels. Isolated-bidirectional dc–dc converters are highly investigated for these applications because their structure naturally meets these two functions. Among all the available topologies, dual active bridge (DAB) isolated-bidirectional dc–dc converters are broadly considered due to their high flexibility and their high efficiency owing to their zero-voltage switching (ZVS) capabilities [2]–[4].

Both single-phase (1p-DAB) [2] and three-phase (3p-DAB) [3] versions are proposed in the literature. Regardless of the higher number of switches, the 3p-DAB provides many advantages over the 1p-DAB which explains why it is preferred in many modern dc-grid applications [5], [6]. The 3p-DAB (see Fig. 1) also allows the use of different winding connections among which the Y-Δ connection has been shown to provide increased performance [7].

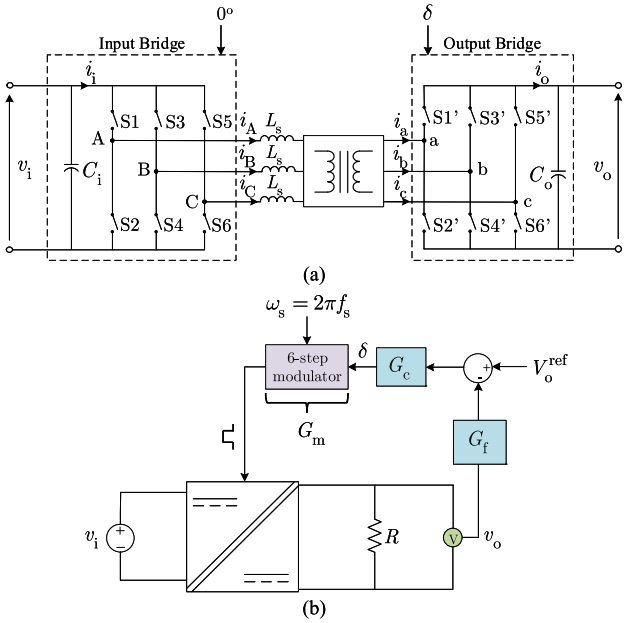

Fig. 1. Three-phase dual active bridge converter. (a) Equivalent circuit of the 3p-DAB topology. (b) Closed-loop structure in the forward operation.

In many dc-grid applications, highly reliable power electronic systems are required to meet a high level of grid-level reliability [8]. Other than a good thermal management, oversizing of components, redundancy of converters, and fault-tolerant (FT) methods are recognized methodologies to improve the reliability of converters. Among these methods, the oversizing of components is the most used in the industry. However, while it may reduce the occurrence of failures, it does not mean that the converter can resume operation upon fault detection.

FT operation is also recognized to be more cost effective than the redundancy approach. FT operation means that a fault in a component or subsystem does not cause the overall system to malfunction [9]. In other words, a degraded operation under postfault conditions implies that the converter can continue operating with reduced performance metrics [10].

Manuscript received April 10, 2019; revised June 26, 2019; accepted July 31, 2019. Date of publication August 5, 2019; date of current version January 10, 2020. Recommended for publication by Associate Editor C. K. Tse. *(Corresponding author: Maxime Berger.)*

M. Berger and I. Kocar are with the Polytechnique Montréal, Montréal, QC H3T 1J4, Canada (e-mail: maxime.berger@polytml.ca; ilhan.kocar@polymtl.ca).

H. Fortin-Blanchette is with the École de Technologie Supérieure, Montréal, QC H3C 1K3, Canada (e-mail: handy.fortin-blanchette@etsmtl.ca).

C. Lavertu is with the Bombardier Transportation, St-Bruno-de-Montarville, QC J3V 6E6, Canada (e-mail: carl.lavertu@rail.bombardier.com).

Color versions of one or more of the figures in this article are available online at http://ieeexplore.ieee.org.

Digital Object Identifier 10.1109/TPEL.2019.2933487

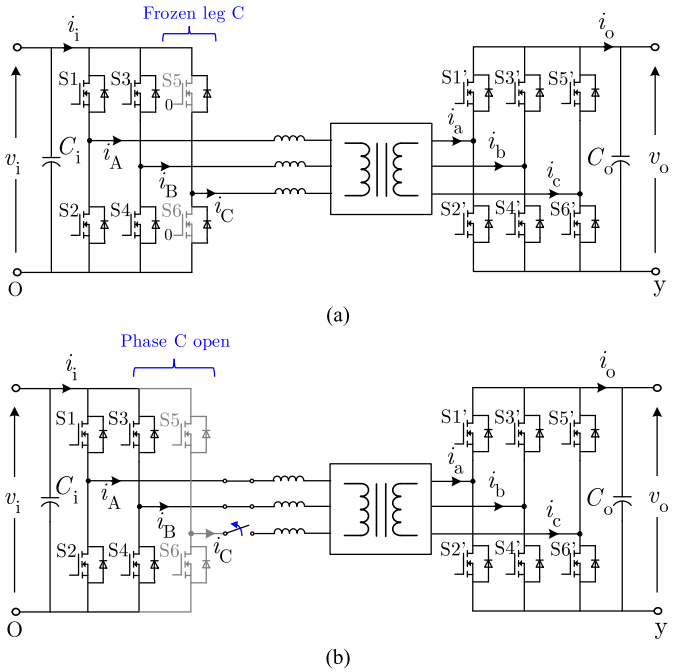

Fig. 2. FT operation of the 3p-DAB. (a) Frozen leg FT operation [11]. (b) Proposed open-phase FT operation.

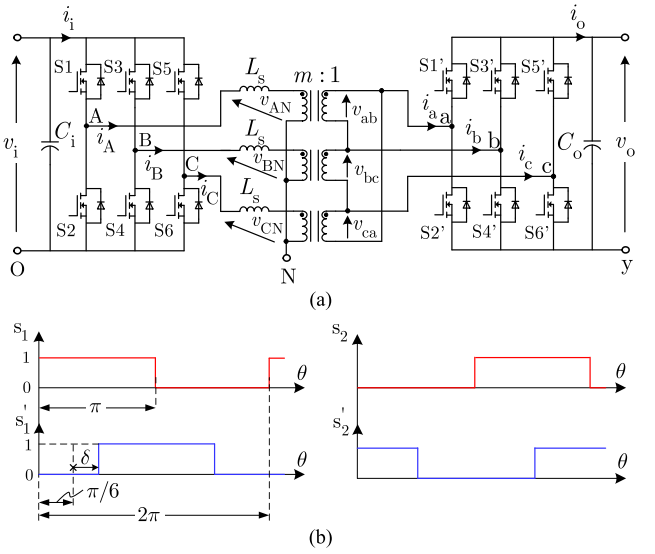

Fig. 3. Additional information on the 3p-DAB version under investigation in this article. (a) Equivalent circuit of the Y-Δ 3p-DAB transformer and definition of the voltage and current variables. (b) Definition of the switching-functions with the control phase-shift δ for phase A. Phases B and C are $\pm 120°$ phase-shifted from phase A.

Because of the higher number of switches in the 3p-DAB, it can be argued that the reliability of the 3p-DAB converter is reduced when compared to other isolated bidirectional dc–dc converter topologies, including the 1p-DAB. However, due to its three-phase structure, it has been shown that the 3p-DAB converter can be operated in a frozen leg degraded mode, i.e., with the two transistors of the same phase being deliberately opened by their gate driver internal protections [see Fig. 2(a)] [11]. Because the free-wheeling diodes are left self-commutated, the analytical characterization of the converter behavior in this degraded mode is not trivial and leads to multiple cases to analyze which are the functions of the converter input/output voltages as well as its loading conditions.

The frozen leg operation of the 3p-DAB leads to increased transformer current as well as a reduced power transfer capability for light and heavier load conditions. These loading conditions are characterized in [11] but are not generalized. Moreover, due to the complexity in deriving an analytical model, the impacts on the ZVS capabilities, controller sizing, dynamic response, and stability are not presented.

In response to this challenge, the research contribution of this article is as follows. First, it is proposed to open the faulty phase on the faulty-bridge side such as it eliminates the interaction of the faulty-leg free-wheeling diodes [see Fig. 2(b)]. As a result, it is possible to characterize the steady state and transient operations of the 3p-DAB with one phase open for all voltage and loading conditions. It allows evaluating the major impacts of the open-phase FT operation as well as presenting key design considerations for a successful open-phase FT operation. Furthermore, the open-phase operation provides increased power transfer capability and reduced circulating current as compared to frozen leg in [11].

This article is, therefore, organized as follows. In Section II, the steady-state analysis based on the piecewise linear modeling approach is performed to characterize the converter in the open-phase operation and evaluate the impacts on the converter steady-state characteristics. The open-phase operation is also compared with frozen leg operation. In Section III, a small-signal frequency-domain analysis is performed to design a suitable closed-loop controller for both normal and open-phase operations as well as to assess the impacts on the converter stability and dynamic performance. Experimental results on a small-scale closed-loop gallium nitride (GaN)-based 3p-DAB prototype and time-domain simulation results are provided to support the theoretical analyses.

Finally, it is worth mentioning that the converter under study is the Y-Δ 3p-DAB version operated using single-phase shift control with a fixed switching frequency f_s and a 180° modulation scheme. The Y-Δ transformer equivalent circuit is shown in Fig. 3(a) and the control phase shift δ is defined in Fig. 3(b). Forward operation is considered such that the output voltage v_o is the regulated variable, as shown in Fig. 1(b). The initial frozen leg condition is assumed to occur on phase C of the input bridge such that phase C is opened in response to the frozen leg gate driver fault signal (see Fig. 2).

II. Steady-State Characterization

The steady-state analysis of the 3p-DAB converter is performed using the piecewise linear modeling approach [3], which can be applied to any transformer connection [7]. The converter

is assumed lossless, and the dead-time is neglected. The transformer magnetizing inductance is also neglected along with transistor snubber and output transistor capacitances. Also note that, throughout this article, small letters are used for time-domain variables while capital letters will be used for the steady-state values.

A. Transformer Voltage and Current Waveforms

The first step to use the piecewise modeling approach to characterize the steady-state operation of the 3p-DAB is to extract the voltage waveforms applied by the input and output bridges on both sides of the series inductance L_s. For the 3p-DAB in the normal operation, the voltages applied by the input bridge on the primary side are given by

$$v_\mathrm{AN} = v_\mathrm{AO} - v_\mathrm{NO} \tag{1}$$

$$v_\mathrm{BN} = v_\mathrm{BO} - v_\mathrm{NO} \tag{2}$$

$$v_\mathrm{CN} = v_\mathrm{CO} - v_\mathrm{NO}. \tag{3}$$

Assuming that the voltages v_AN, v_BN, and v_CN are balanced, and adding (1)–(3), it leads to

$$v_\mathrm{NO} = \frac{v_\mathrm{AO} + v_\mathrm{BO} + v_\mathrm{CO}}{3} \tag{4}$$

with

$$v_\mathrm{AO} = \mathrm{s}_1 v_\mathrm{i} \tag{5}$$

$$v_\mathrm{BO} = \mathrm{s}_3 v_\mathrm{i} \tag{6}$$

$$v_\mathrm{CO} = \mathrm{s}_5 v_\mathrm{i} \tag{7}$$

and s_1 being the switching function of phase A defined in Fig. 3(b). The switching functions s_3 and s_5 are $\pm$ 120° phase-shifted from phase A. Inserting (5)–(7) into (4), it yields that

$$v_\mathrm{NO} = \frac{(\mathrm{s}_1 + \mathrm{s}_3 + \mathrm{s}_5)\, v_\mathrm{i}}{3}. \tag{8}$$

From (8), it is concluded that the voltage v_NO, on the primary side, only depends on the input bridge switching functions and the converter input voltage. Furthermore, inserting (5)–(8) into (1)–(3) leads to

$$v_\mathrm{AN} = \frac{(2\mathrm{s}_1 - \mathrm{s}_3 - \mathrm{s}_5)\, v_\mathrm{i}}{3} \tag{9}$$

$$v_\mathrm{BN} = \frac{(2\mathrm{s}_3 - \mathrm{s}_1 - \mathrm{s}_5)\, v_\mathrm{i}}{3} \tag{10}$$

$$v_\mathrm{CN} = \frac{(2\mathrm{s}_5 - \mathrm{s}_1 - \mathrm{s}_3)\, v_\mathrm{i}}{3}. \tag{11}$$

A similar analysis can be carried out on the secondary side,

$$v'_\mathrm{ab} = m v_\mathrm{ab} = m\,(\mathrm{s}'_1 - \mathrm{s}'_3)\, v_\mathrm{o} \tag{12}$$

$$v'_\mathrm{bc} = m v_\mathrm{bc} = m\,(\mathrm{s}'_3 - \mathrm{s}'_5)\, v_\mathrm{o} \tag{13}$$

$$v'_\mathrm{ca} = m v_\mathrm{ca} = m\,(\mathrm{s}'_5 - \mathrm{s}'_1)\, v_\mathrm{o} \tag{14}$$

with s'_1, s'_3, and s'_5 being the output bridge switching functions for phase a, b, and c, respectively. Knowing the voltages applied to the series inductor, the phase currents can be defined for the interval from 0 to π following the procedure given in [3]. For the 3p-DAB, the application of the piecewise linear modeling approach is divided into two ranges depending on the control phase shift δ. For the specific case of the Y-Δ 3p-DAB under investigation, range 1 is defined as $0 \leq \delta \leq \pi/6$ and range 2 is defined as $\pi/6 \leq \delta \leq \pi/2$. Also note that in the normal operation, the three-phase currents are assumed balanced

$$i_\mathrm{A} + i_\mathrm{B} + i_\mathrm{C} = 0. \tag{15}$$

In the open-phase operation, the voltage waveforms are affected and differ from the normal case. If phase C is open, the current in phase C is null. Knowing that the voltage across L_s on phase C is also null, it can be concluded that the voltage v_CN is now a function of the output voltage v_o. Therefore, following (14), the new voltage v_CN in the open-phase mode is as follows:

$$v_\mathrm{CN} = m v_\mathrm{ca} = m\,(\mathrm{s}'_5 - \mathrm{s}'_1)\, v_\mathrm{o}. \tag{16}$$

If the output bridge is still operated with the same balanced set of switching functions, it can be said that

$$v_\mathrm{ab} + v_\mathrm{bc} + v_\mathrm{ca} = 0 \tag{17}$$

such that v_AN, v_BN, and v_CN remain balanced, and (4) still stands in the open-phase operation. While (5) and (6) still apply for the open-phase operation, the voltage v_CO is not applied by the input bridge since phase C is open, such that, the following general relationship must now be considered:

$$v_\mathrm{CO} = v_\mathrm{CN} + v_\mathrm{NO}. \tag{18}$$

Inserting (5), (6), and (18) into (4), with v_CN given by (16), the voltage v_NO for the open-phase operation is reduced to

$$v_\mathrm{NO} = \frac{(\mathrm{s}_1 + \mathrm{s}_3)\, v_\mathrm{i} + m\,(\mathrm{s}'_5 - \mathrm{s}'_1)\, v_\mathrm{o}}{2}. \tag{19}$$

By inserting (19) into (1) and (2), the new voltages v_AN and v_BN are defined by

$$v_\mathrm{AN} = \frac{(\mathrm{s}_1 - \mathrm{s}_3)\, v_\mathrm{i} + m\,(\mathrm{s}'_1 - \mathrm{s}'_5)\, v_\mathrm{o}}{2} \tag{20}$$

$$v_\mathrm{BN} = \frac{(\mathrm{s}_3 - \mathrm{s}_1)\, v_\mathrm{i} + m\,(\mathrm{s}'_1 - \mathrm{s}'_5)\, v_\mathrm{o}}{2}. \tag{21}$$

The results obtained in (20) and (21) lead to an important conclusion. In the open-phase operation, the voltages v_AN and v_BN are dependent on the output bridge switching functions and the output voltage v_o. This is a fundamental difference compared to the normal operation.

In the open-phase operation, (15) is also still applicable, which leads to the other important conclusion that the phase A and B currents are still purely ac, but now out of phase

$$i_\mathrm{A} = -i_\mathrm{B}. \tag{22}$$

For the same input and output voltages as well as loading conditions, experimental waveforms for phase A are provided to compare the normal (see Fig. 4) and open-phase (see Fig. 5) operations. This test case will be used as the main example for the remaining of this article. The main parameters of the experimental prototype are provided in Table I. The experimental prototype is shown in Fig. 6.

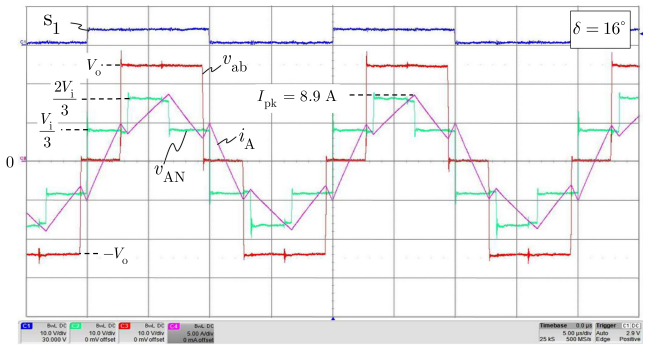

Fig. 4. Main test case experimental results for the transformer voltage and current waveforms for phase A in normal operation. The converter is operated in range 1.

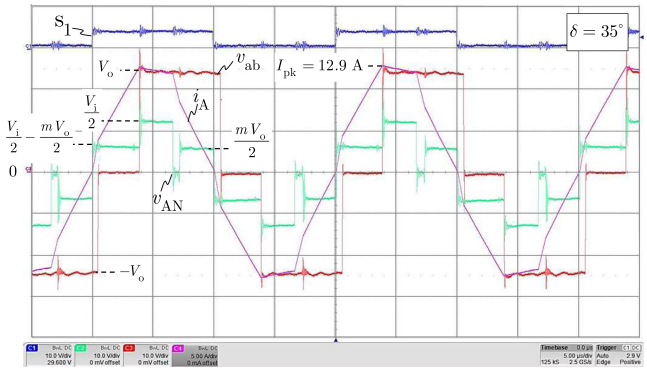

Fig. 5. Main test case experimental results for the transformer voltage and current waveforms for phase A with phase C open. The converter is operated in range 2.

TABLE I
EXPERIMENTAL PROTOTYPE MAIN TEST CASE PARAMETERS

Description	Symbol	Value
Input and Output Voltage	V_i, V_o	24 V
Load Resistance	R	4 Ω
Output Capacitor	C_i, C_o	164 µF
Series Inductance	L_s	2 µH
Transformer Ratio	m:1	0.5 : 1
Switching Frequency	f_s	50 kHz

A similar analysis can be performed on the secondary side. In this case, it is the secondary voltage waveforms v'_{ab}, v'_{bc}, and v'_{ca} that are modified instead of v_{AN}, v_{BN}, and v_{CN}. For example, if phase c is opened on the secondary side, the voltage v'_{ab} remains the same as in the normal operation but v'_{bc} and v'_{ca} will depend on the input voltage v_i due to coupling with the voltages applied by the input bridge on the primary side of the three-phase transformer.

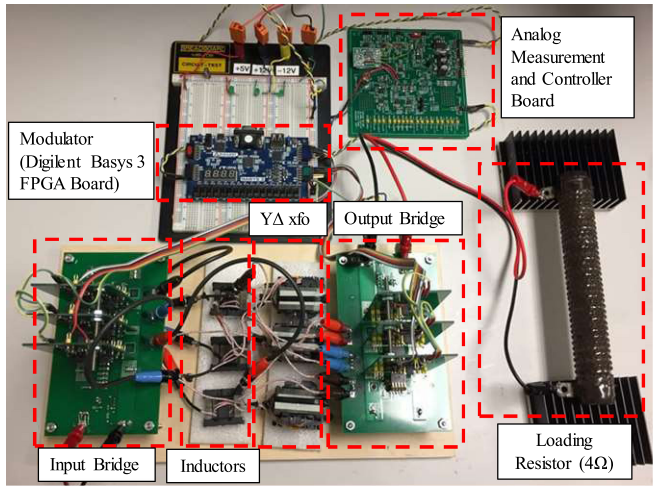

Fig. 6. EPC2022 GaN-based 3p-DAB experimental prototype with the Y-Δ transformer. Open-phase operation is studied by opening the connection between the phase C inductor and the input bridge.

B. Power Transfer Relationship

The general procedure to derive the power transfer relationship of the 3p-DAB in the normal operation has been presented in [3]. It assumes constant dc voltages and the steady-state operation. It requires averaging the input or output currents which are expressed in terms of the transformer line currents as well as the input and output bridge switching functions. Due to the symmetrical operation of the 3p-DAB in the normal operation, the analysis is only performed over the interval $\theta = [0, \pi/3]$. For the Y-Δ 3p-DAB, the power transfer relationships for ranges 1 and 2 are given, respectively, by

$$P = \frac{mV_\mathrm{i}V_\mathrm{o}}{\omega_\mathrm{s}L_\mathrm{s}}\delta \tag{23}$$

$$P = \frac{mV_\mathrm{i}V_\mathrm{o}}{\omega_\mathrm{s}L_\mathrm{s}}\left[\frac{3}{2}\left(\delta - \frac{\delta^2}{\pi}\right) - \frac{\pi}{24}\right]. \tag{24}$$

The analysis of the 3p-DAB in open-phase requires to analyze the transformer currents over the longer interval $\theta = [0, \pi]$ because of the unbalanced operation. It can be demonstrated that the resulting power transfer capability is theoretically half of the one in the normal operation.

For the experimental prototype parameters, the power transfer relationships in the normal, frozen leg, and open-phase operations are compared in Fig. 7. Experimental results are included to validate the theoretical models. As depicted in Fig. 7, when the converter is operated in a closed loop with regulated output voltage $v_\mathrm{o} = V_\mathrm{o}$ and a resistive load R, the output power P_o must remain constant such that in the frozen leg and open-phase conditions, the control phase shift δ will naturally be increased to meet the new operating conditions.

Due to the circulation of reactive current in the faulty phase free-wheeling diodes in the frozen leg operation, the power transfer capability is reduced as compared to open-phase. However, for conditions where there is no reactive current circulating in

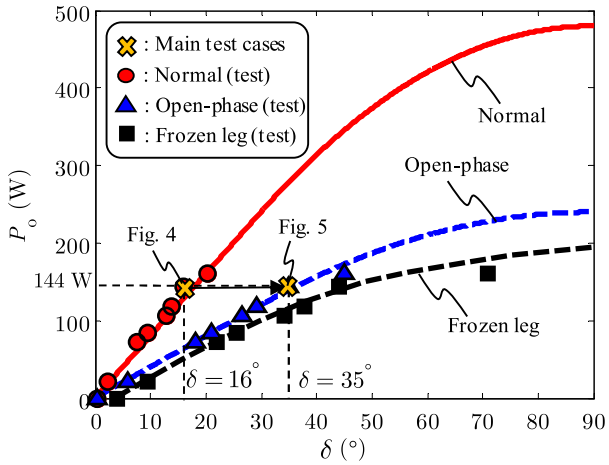

Fig. 7. Comparison of the theoretical and experimental power transfer relationships for the prototype parameters. For the frozen leg mode, the theoretical power transfer capability is evaluated using time-domain simulations because of the analytical complexity. The errors between the theoretical and the experimental results are mainly due to losses and the dead-time (0.1 μs) which are not considered in the theoretical models. As the power increases, losses reduce the accuracy of the theoretical models for the open-phase and frozen leg modes. The power transfer capability is also smaller than expected by the theoretical prediction. Note that the 3p-DAB is also rarely operated with phase-shift beyond 60° due to the important circulation of reactive power [12].

the faulty phase, the frozen leg operation is virtually equivalent to the open-phase operation.

C. Current Stress

Fig. 8 shows the current for each phase in the faulty bridge for different voltage and loading conditions. These results are obtained from time-domain simulations. Experimental results are also added. The voltage conversion ratio d is defined as

$$d = \frac{V_\mathrm{i}}{mV_\mathrm{o}}. \tag{25}$$

By analyzing the results for the currents in phase A and phase B, it is concluded that the current stress on the switches is higher in the frozen leg operation as compared to the open-phase case due to reactive currents circulating in the faulty phase C in the frozen leg operation. This advantage of open-phase over frozen leg also increases as d decreases.

Moreover, it is remarked that the rms current in phase A and phase B is generally higher in the frozen leg and open-phase operations as compared to the normal operation. This is an intuitive result since the total active power is transmitted through the two remaining phases in the frozen leg and open-phase operations. For low power, it can, however, be noted that the rms current in phase A and phase B can be lower in the frozen leg and open-phase operations as compared to the normal operation. This is a counterintuitive result since the total active power is transmitted through the remaining phases, but this is due to modifications in the voltage and current waveforms as described in Section II-A.

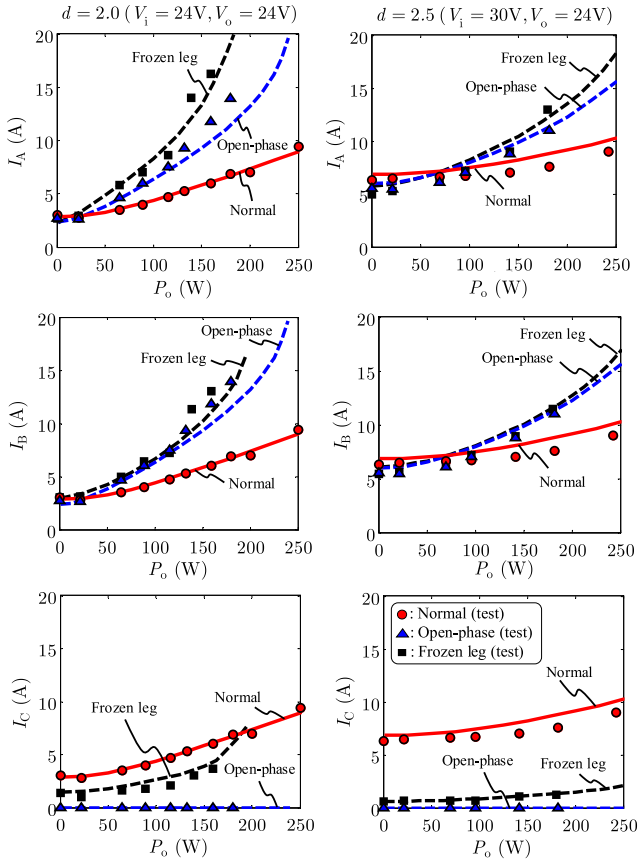

Fig. 8. Analysis of the rms current stress in the faulty bridge for different voltage and loading conditions with time-domain simulations and experimental tests.

D. ZVS Soft-Switching Regions

The 3p-DAB make use of reactive circulating current through the transistor antiparallel diodes of each bridge to provide ZVS at turn-ON. ZVS occurs in the input bridge if $i_\mathrm{A} < 0$ at turn-ON of S1, and ZVS occurs in the output bridge if $i_\mathrm{a} > 0$ at turn-ON of S1′. The procedure to evaluate the theoretical ZVS regions for the 3p-DAB in the normal operation has been presented in [3] and [7]. The results for the Y-Δ 3p-DAB in the normal operation are given in Fig. 9(a). A similar procedure can be applied in the open-phase operation, but since the currents are unbalanced, each phase must be studied independently. The analysis for phase A (input bridge) and phase a (output bridge) is shown in Fig. 9(b).

The theoretical results in Fig. 9 are also compared with the main test case experimental results. As expected for the normal operation case in Fig. 4 ($i_\mathrm{A} < 0$ at turn-ON of S1), the input bridge is soft switched in Fig. 9(a). Since it is operated far from its hard-switching boundary, the reactive component of i_A is significant (see Fig. 4). In the open-phase operation, according to Fig. 9(b), the phase A of the input bridge should be soft switched but operated very close to its ZVS boundary. According to Fig. 5, i_A is close to zero at turn-ON of S1 which means that it is operated close to its ZVS boundary.

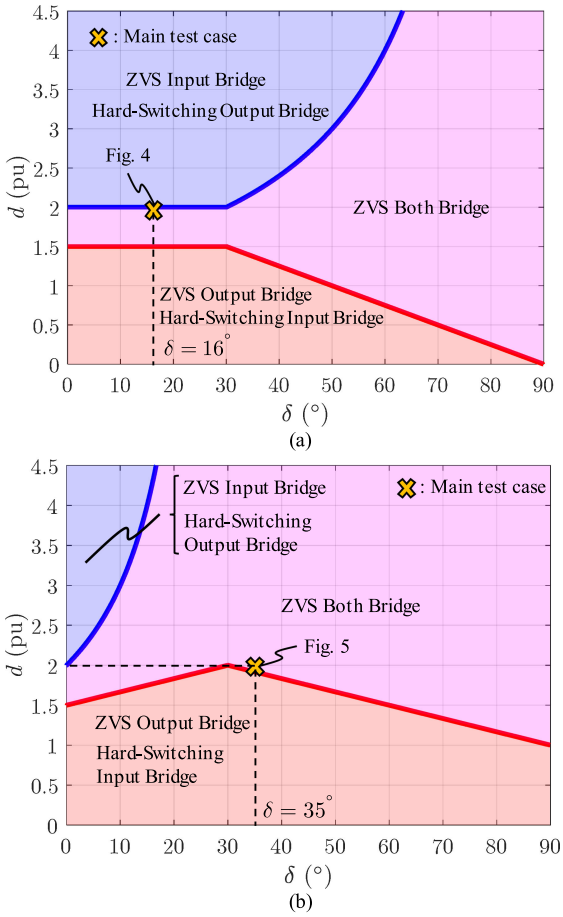

Fig. 9. ZVS regions. (a) Normal operation. (b) Open-phase operation (phase A and phase a).

The results in Fig. 9(a) show that it is advantageous from a soft-switching standpoint to operate the 3p-DAB in the normal operation with a voltage conversion ratio d ranging between 1.5 and 2. It is possible in applications where the input voltage V_i is tightly regulated by a preregulating stage and the output voltage V_o is held constant by the DAB converter. Type D multistage solid-state transformers [13] such as those presented in [14] and [15] are potential candidates. In fact, if the input voltage V_i is well regulated, it is possible to select the transformer ratio m such as the voltage conversion ratio d always lies between 1.5 and 2.0 for a desired fixed output voltage V_o.

In open-phase, a similar analysis can be performed for the other phases. In fact, ZVS happens in phase B of the input bridge if $i_\mathrm{B} < 0$ at turn-ON of S3, and ZVS take place in phase b of the output bridge if $i_\mathrm{b} > 0$ at turn-ON of S3′. Since phase C is open, the ZVS analysis is not applicable for phase C of the input bridge but ZVS occurs in phase c of the output bridge if $i_\mathrm{c} > 0$ at turn-ON of S5′. Since $i_\mathrm{A} = -i_\mathrm{B}$ and $i_\mathrm{C} = 0$, the output bridge currents i_a, i_b, and i_c can all be derived from the knowledge of i_A. It results that $i_\mathrm{a} = i_\mathrm{c} = mi_\mathrm{A}$ and $i_\mathrm{b} = -2mi_\mathrm{A}$ which simplifies the ZVS analysis for the other phases.

Based on the above methodology, a detailed analysis of the relationship between the output power P_o, the conversion ratio d and the ZVS boundaries is provided for all phases in Fig. 10.

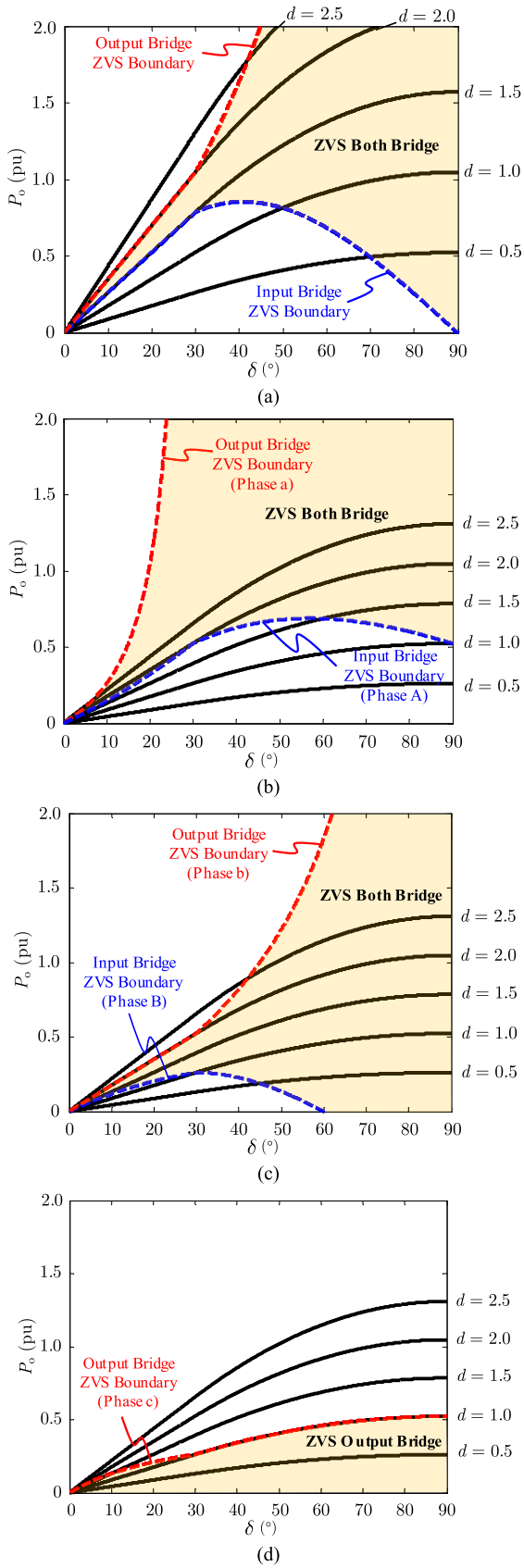

Fig. 10. Output power versus the control phase-shift with the conversion ratio d as a parameter. (a) Normal. (b) Open-phase (phase A and phase a). (c) Open-phase (phase B and phase b). (d) Open-phase (phase c).

For the per-unit conversion, the following bases are taken:

$$V_{\rm b} = mV_{\rm o},\ P_{\rm b} = \frac{(mV_{\rm o})^2}{\omega_{\rm s}L_{\rm s}}. \tag{26}$$

For the normal case, the results in Fig. 10(a) are valid for all phases. In the open-phase operation, the results are given in Fig. 10(b)–(d). From these results, it is concluded that in the open-phase operation, for $d = 2$, the input bridge is always ZVS, but only phase a and phase b in the output bridge are ZVS. The whole output bridge is also always ZVS for a voltage conversion ratio $d < 1$.

E. Impacts of Open-Phase on Magnetics

The impacts of the open-phase operation on magnetics are discussed here. The three-phase transformer can either be constructed with all the windings on a single core or using three separate transformers. Moreover, the series inductance $L_{\rm s}$ can be implemented by adding external inductors or it can be integrated into the transformer by controlling the leakage inductance of the three phases [12].

If external inductors are used, their core must be correctly sized for the maximum peak current $i_{\rm pk}$ which increases in the open-phase operation for the same voltage and loading conditions. For example, for the main test case parameters, the peak current increases from 8.9 A in the normal operation (see Fig. 4) to 12.9 A in the open-phase operation (see Fig. 5). This increase in the peak current must be considered during design to avoid core saturation of the inductors in the open-phase operation.

For the three-phase transformer, the winding conductors must be correctly sized for the increased rms current in the open-phase operation. Furthermore, from the analysis of Figs. 4 and 5, it is concluded that the volt-seconds applied to the transformer magnetizing inductance is not affected in the open-phase operation because the healthy output bridge continues applying the same voltage waveforms to the transformer secondary windings. Thus, the risk of the transformer saturation does not increase in the open-phase operation. Since there is no dc component in the phase current in the open-phase operation, this also means that the balance of volt-seconds applied to the transformer leakage inductance is maintained.

III. Small-Signal and Transient Analyses

A. Derivation of the Small-Signal Model

Converter open loop small-signal characteristics are generally defined by a set of standard transfer functions: the control-to-output transfer function $G_{\rm vd}(s)$, the line-to-output transfer function $G_{\rm vg}(s)$, and the input $Z_{\rm i}(s)$ and output $Z_{\rm o}(s)$ impedances [16], [17]. The control-to-output transfer function $G_{\rm vd}(s)$ is necessary to properly size the closed-loop controller $G_c(s)$ (see Fig. 1). While $G_{\rm vg}(s)$ is important for electromagnetic compatibility analysis, $Z_{\rm i}(s)$ and $Z_{\rm o}(s)$ are widely used in practice for the application of impedance-based stability criteria [18]–[20].

The most commonly used technique to derive the analytical small-signal model of dc–dc converters is the state-space averaging (SSA) method [21]–[23]. The resulting SSA small-signal circuits for the Y-Δ 3p-DAB in the normal and open-phase operations are shown in Fig. 11. For the 3p-DAB in the normal and the open-phase operations, it leads to the following general form of the transfer function $G_{\rm vd}(s)$:

$$G_{\rm vd}(s) = \frac{K_{\rm vd}}{sRC_{\rm o} + 1} \tag{27}$$

with $K_{\rm vd}$ being given in Table II and being dependent on both the operating range and the operating mode. By analyzing (27), it is first concluded that the phase of $G_{\rm vd}(s)$ is not affected in the open-phase operation. However, from Table II, it is concluded that the gain $K_{\rm vd}$ in range 1 is half the gain in the normal operation. While it may look that it is also the case in range 2, the gain $K_{\rm vd}$ depends on the control phase shift δ, which, as previously mentioned, for the same input and output voltages as well as loading conditions, must increase in the open-phase condition (see Fig. 7). For the main test case parameters (see Figs. 4 and 5), the magnitude of $G_{\rm vd}(s)$ for both modes is also compared in Fig. 12.

TABLE II
Control-to-Output Transfer Functions Gain $K_{\rm vd}$

	Normal	Open-Phase
Range 1	$K_{\rm vd} = \dfrac{mRV_{\rm i}}{\omega_{\rm s}L_{\rm s}}$	$K_{\rm vd} = \dfrac{mRV_{\rm i}}{2\omega_{\rm s}L_{\rm s}}$
Range 2	$K_{\rm vd} = \dfrac{mRV_{\rm i}}{\omega_{\rm s}L_{\rm s}}\left[\dfrac{3}{2}\left(1-\dfrac{2\delta}{\pi}\right)\right]$	$K_{\rm vd} = \dfrac{mRV_{\rm i}}{2\omega_{\rm s}L_{\rm s}}\left[\dfrac{3}{2}\left(1-\dfrac{2\delta}{\pi}\right)\right]$

While SSA is used here because it gives a better insight of system parameters sensitivity, it is, however, shown in [16] that it has limitations in deriving an accurate small-signal model of the 3p-DAB at frequencies higher than 1/5th of the switching frequency f_s. SSA is generally precise enough for controller sizing with $G_{\rm vd}(s)$ and for the evaluation of $Z_{\rm o}(s)$, but it lacks precision for the evaluation of $G_{\rm vg}(s)$ and $Z_{\rm i}(s)$.

To overcome the limitations of SSA for DAB converters, the generalized state-space averaging (GSSA) approach is used [24]–[27]. In the open-phase operation, since the primary voltages $v_{\rm AN}$ and $v_{\rm BN}$ both depend on the output bridge switching functions as well as the output voltage $v_{\rm o}$, the derivation of the GSSA model requires to rewrite the converter differential equations. The procedure to derive the GSSA model with the index $k = 0$ terms of $v_{\rm i}$, $i_{\rm i}$, and $v_{\rm o}$ and the index $k = \pm 1$ terms of $i_{\rm A}$ and $i_{\rm B}$ is adapted from [16] and [24]–[27]. It leads to the following formulation:

$$\frac{d\left\langle \hat{\mathbf{x}}(t)\right\rangle}{dt} = \hat{\mathbf{A}}\left\langle \hat{\mathbf{x}}(t)\right\rangle + \hat{\mathbf{B}}\left\langle \hat{\mathbf{u}}(t)\right\rangle \tag{28}$$

$$\left\langle \hat{\mathbf{y}}(t)\right\rangle = \hat{\mathbf{C}}\left\langle \hat{\mathbf{x}}(t)\right\rangle + \hat{\mathbf{D}}\left\langle \hat{\mathbf{u}}(t)\right\rangle \tag{29}$$

with the averaged vectors of state variables, and input and output defined as

$$\left\langle \hat{\mathbf{x}}\right\rangle = \left[\left\langle \hat{v}_{\rm o}\right\rangle_0 \left\langle \hat{i}_{\rm A}\right\rangle_1^{\rm R} \left\langle \hat{i}_{\rm A}\right\rangle_1^{\rm I} \left\langle \hat{i}_{\rm B}\right\rangle_1^{\rm R} \left\langle \hat{i}_{\rm B}\right\rangle_1^{\rm I}\right]^T \tag{30}$$

$$\left\langle \hat{\mathbf{u}}\right\rangle = \left[\hat{\delta}\ \left\langle \hat{v}_{\rm i}\right\rangle_0\right]^T,\ \left\langle \hat{\mathbf{y}}\right\rangle = \left[\left\langle \hat{v}_{\rm o}\right\rangle_0 \left\langle \hat{i}_{\rm i}\right\rangle_0\right]^T \tag{31}$$

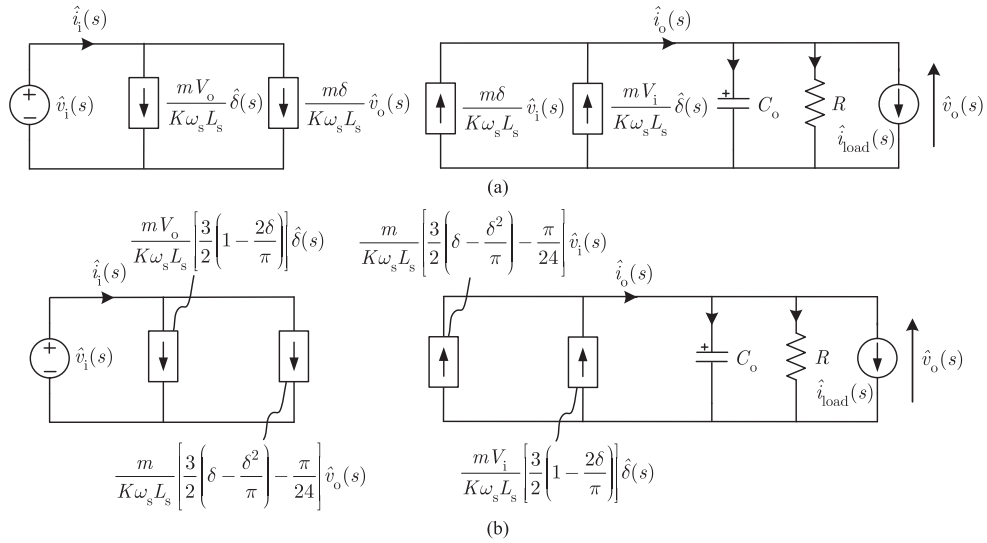

Fig. 11. Equivalent SSA small-signal circuits of the Y-Δ 3p-DAB converter. (a) Range 1. (b) Range 2. For the normal operation $K = 1$, and for the open-phase operation $K = 2$. These equivalent circuits are used in this article to determine $G_{\rm vd}(s)$, $G_{\rm vg}(s)$, and $Z_{\rm i}(s)$ with SSA.

and the averaged state-space matrices defined as

$$\hat{\mathbf{A}} = \begin{bmatrix} \frac{-1}{RC_{\rm o}} & A_{12} & A_{13} & A_{14} & A_{15} \\ A_{21} & 0 & \omega_{\rm s} & 0 & 0 \\ A_{31} & -\omega_{\rm s} & 0 & 0 & 0 \\ A_{41} & 0 & 0 & 0 & \omega_{\rm s} \\ A_{51} & 0 & 0 & -\omega_{\rm s} & 0 \end{bmatrix}, \ \hat{\mathbf{B}} = \begin{bmatrix} B_{11} & 0 \\ B_{21} & \frac{\sqrt{3}}{4\pi L_{\rm s}} \\ B_{31} & \frac{-3}{4\pi L_{\rm s}} \\ B_{41} & \frac{-\sqrt{3}}{4\pi L_{\rm s}} \\ B_{51} & \frac{3}{4\pi L_{\rm s}} \end{bmatrix} \tag{32}$$

$$\hat{\mathbf{C}} = \begin{bmatrix} 1 & 0 & 0 & 0 & 0 \\ 0 & 0 & -\frac{2}{\pi} & -\frac{\sqrt{3}}{\pi} & \frac{1}{\pi} \end{bmatrix}, \ \hat{\mathbf{D}} = \begin{bmatrix} 0 & 0 \\ 0 & 0 \end{bmatrix}. \tag{33}$$

The $\hat{\mathbf{A}}$ matrix terms are given as follows:

$$A_{12} = \frac{2S_{12}}{C_{\rm o}}, \ A_{13} = \frac{2S_{13}}{C_{\rm o}}, \ A_{14} = \frac{2S_{14}}{C_{\rm o}}, \ A_{15} = \frac{2S_{15}}{C_{\rm o}} \tag{34}$$

with

$$\begin{aligned} S_{12} &= \frac{m}{\pi}\left[\sin\left(\frac{7\pi}{6}+\delta\right) - \sin\left(\frac{11\pi}{6}+\delta\right)\right] \\ S_{13} &= \frac{m}{\pi}\left[\cos\left(\frac{7\pi}{6}+\delta\right) - \cos\left(\frac{11\pi}{6}+\delta\right)\right] \\ S_{14} &= \frac{m}{\pi}\left[\sin\left(\frac{11\pi}{6}+\delta\right) - \sin\left(\frac{\pi}{2}+\delta\right)\right] \\ S_{15} &= \frac{m}{\pi}\left[\cos\left(\frac{11\pi}{6}+\delta\right) - \cos\left(\frac{\pi}{2}+\delta\right)\right] \end{aligned} \tag{35}$$

and

$$A_{21} = \frac{-S_{21}}{L_{\rm s}}, \ A_{31} = \frac{-S_{31}}{L_{\rm s}}, \ A_{41} = \frac{S_{41}}{L_{\rm s}}, \ A_{51} = \frac{S_{51}}{L_{\rm s}} \tag{36}$$

$$\begin{aligned} S_{21} = S_{41} &= \frac{m}{2\pi}\left[\sin\left(\frac{7\pi}{6}+\delta\right) - 3\sin\left(\frac{11\pi}{6}+\delta\right)\right] \\ S_{31} = S_{51} &= \frac{m}{2\pi}\left[\cos\left(\frac{7\pi}{6}+\delta\right) - \cos\left(\frac{11\pi}{6}+\delta\right)\right]. \end{aligned} \tag{37}$$

The $\hat{\mathbf{B}}$ matrix terms are given as follows:

$$B_{21} = \frac{-S_{31}\mathrm{V_o}}{L_{\rm s}}, \ B_{31} = \frac{S_{21}\mathrm{V_o}}{L_{\rm s}}, \\ B_{41} = \frac{S_{31}\mathrm{V_o}}{L_{\rm s}}, \ B_{51} = \frac{-S_{21}\mathrm{V_o}}{L_{\rm s}} \tag{38}$$

$$B_{11} = \frac{2}{C_{\rm o}}\sum_{n=1}^{4} B_{11}(n) \tag{39}$$

with the $B_{11}(n)$ terms being defined as

$$\begin{aligned} B_{11}(1) &= S_{13}\langle I_{\rm A}\rangle_1^{\rm R}, \ B_{11}(2) = -S_{12}\langle I_{\rm A}\rangle_1^{\rm I} \\ B_{11}(3) &= S_{15}\langle I_{\rm B}\rangle_1^{\rm R}, \ B_{11}(4) = -S_{14}\langle I_{\rm B}\rangle_{1.}^{\rm I} \end{aligned} \tag{40}$$

B. Analysis of the Converter Transfer Functions

The impacts of the open-phase operation on the small-signal characteristics of the 3p-DAB also need to be analyzed. The main test case parameters (see Figs. 4 and 5) are used and the magnitude of $G_{\rm vd}(s)$, $G_{\rm vg}(s)$, and $Z_{\rm i}(s)$ are shown in Figs. 12–14. Time-domain simulation results are also added to validate the normal and open-phase operation models.

First, from Figs. 13 and 14, it is concluded that the use of SSA leads to the false conclusion that for the same input and output voltages as well as loading conditions, the transfer functions $G_{\rm vg}(s)$ and $Z_{\rm i}(s)$ are not affected in the open-phase operation. In the open-phase operation, the magnitude of $G_{\rm vg}(s)$ tends, in fact to decrease at higher frequencies (see Fig. 13). For $Z_{\rm i}(s)$, the peak gain frequency is shifted from 1.8 to 2.5 kHz in

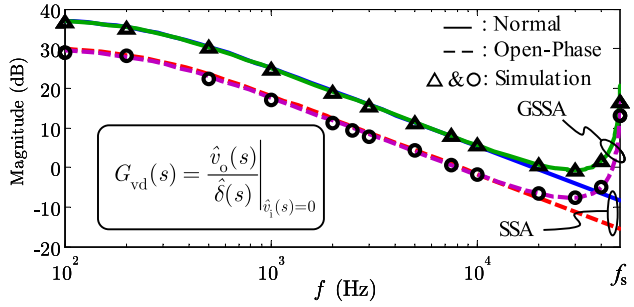

Fig. 12. Magnitude of the control-to-output transfer function $G_{vd}(s)$.

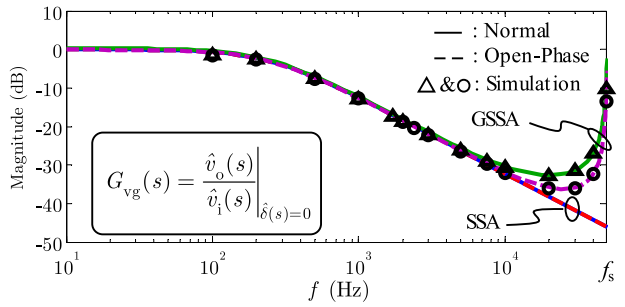

Fig. 13. Magnitude of the line-to-output transfer function $G_{vg}(s)$.

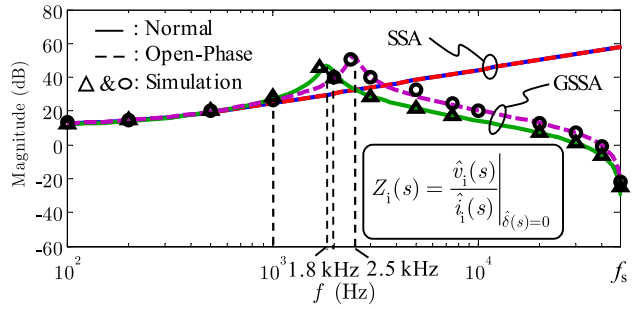

Fig. 14. Magnitude of the input impedance $Z_i(s)$.

the open-phase operation. According to Middlebrook's theorem [18], for a given input filter, it tends to be less stable between 1 and 2 kHz but to be more stable at frequencies higher than 2 kHz (see Fig. 14).

Since the output impedance only depends on the load R and the output capacitor C_o, it is not affected in the open-phase operation such that $Z_o(s)$ can be calculated as defined in [16].

C. Closed-Loop Analysis in the Open-Phase Operation

When switching from the normal to open-phase operation with the same input and output voltages as well as loading conditions, it must be determined if the controller parameters need to be adjusted to keep an acceptable transient dynamic response.

To answer this question, a PI controller G_c is sized here using the transfer function G_{vd} of the 3p-DAB in the normal operation (see Fig. 12). The characteristics of the designed PI controller G_c are given in Fig. 15. This controller is used

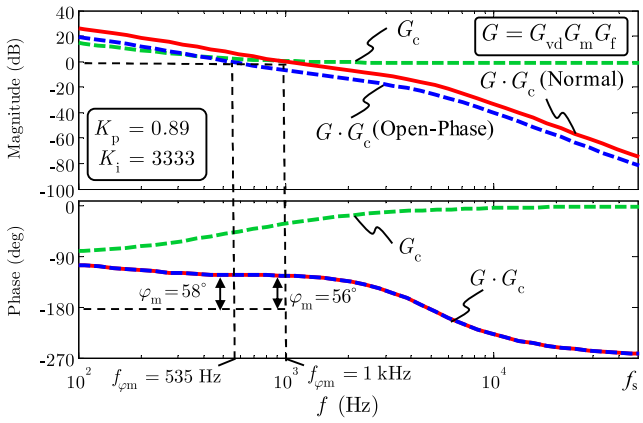

Fig. 15. Impact of sizing the controller using normal operation characteristics on the closed-loop small-signal characteristics in the open-phase operation.

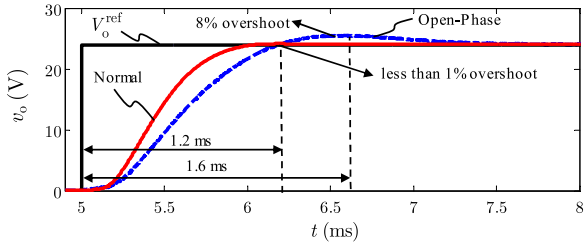

Fig. 16. Time-domain simulation results showing the impact of sizing the controller using the converter normal operation characteristics on the transient response in the open-phase operation.

for both simulation and experimental analyses. The impacts of keeping the same controller G_c when passing from the normal to open-phase operation on the crossover frequency $f_{\varphi m}$ and the phase margin φ_m are also given in Fig. 15. Overall, it is concluded that the crossover frequency $f_{\varphi m}$ is reduced from 1 kHz in the normal operation to 535 Hz in the open-phase operation. The phase-margin φ_m is slightly increased from 56° to 58°.

By applying a step from 0 to 24 V in the reference voltage in the time-domain simulation model, it is seen in Fig. 16 that the overall result is a higher overshoot (8% against less than 1%) and a slower transient response (time-to-peak of 1.6 ms against 1.2 ms). This is due to the reduced ability of the same PI controller G_c to deal with disturbances in open-phase. This is mainly due to the important reduction in the crossover frequency $f_{\varphi m}$. This situation can be considered acceptable in some practical applications, but the controller parameters may need to be adjusted in some cases.

The experimental results of Fig. 17 also show that the simulation model provides a reasonable accuracy in predicting the transient response in open-phase. Furthermore, the simulation results in Fig. 18 show that the designed controller allows a transition from the normal to frozen leg and from the frozen leg to open-phase without interruption. From Fig. 18, for the same output power, it is also concluded that the open-phase operation provides reduced current stress and an increased power transfer

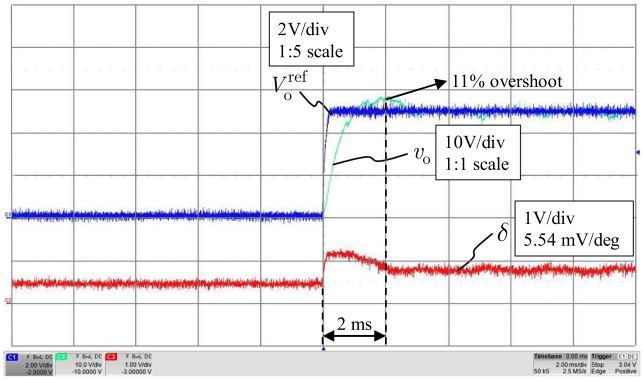

Fig. 17. Closed-loop transient response to a step in the reference voltage from 0 to 24 V for the open-phase operation.

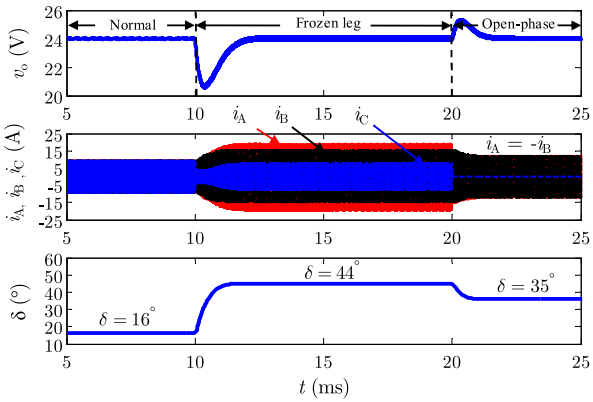

Fig. 18. Time-domain simulation results for the closed-loop transition from normal to frozen leg and from frozen leg to open-phase operations.

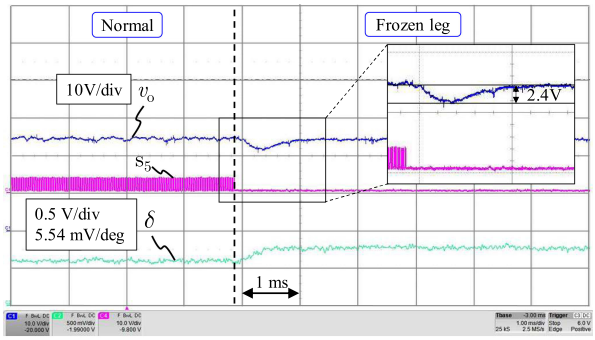

Fig. 19. Experimental results for the transition from normal to frozen leg. The result is close to the simulation result in Fig. 18.

capability over the frozen leg operation (i.e., the phase shift δ is smaller in open-phase than in frozen leg).

Moreover, experimental results also confirm that the designed controller allows uninterrupted transitions from the normal to frozen leg (see Fig. 19), from the frozen leg to open-phase (see Fig. 20), and from the normal to open-phase (see Fig. 21). The normal to frozen leg transition is performed by disabling the phase C gating signals s_5 and s_6. The frozen leg to open-phase and the normal to open-phase transitions are validated by opening the normally closed (NC) contact of a relay inserted in the

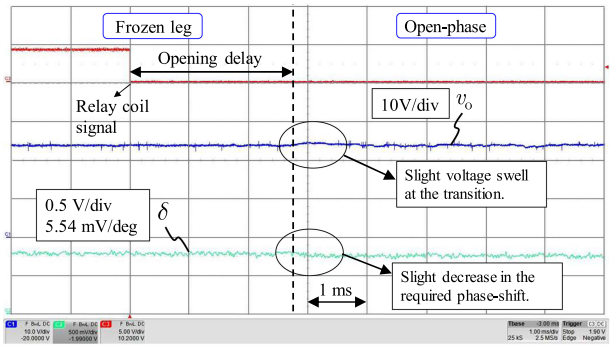

Fig. 20. Experimental results for the transition from frozen leg to open-phase. The result is close to the simulation result in Fig. 18.

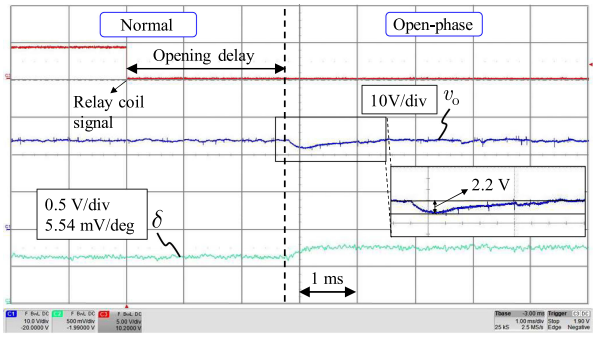

Fig. 21. Experimental results for the transition from normal to open-phase. A voltage dip of 2.2 V is observed during the transition.

phase C. The relay coil signal is used to trigger the oscilloscope and capture the event. A delay of 2.8 ms between the coil opening signal and the actual phase opening is introduced by the relay.

IV. Discussion on Fault Diagnosis and Remedial Actions for Open-Phase FT Operation

FT operation relies on effective fault diagnosis (FD) methodologies and adequate remedial actions [10]. As demonstrated in this article, the 3p-DAB is naturally tolerant to phase loss (PL) type fault (e.g., loose connection or broken wire). In this case, if the controller is correctly sized, the 3p-DAB directly falls from the normal to open-phase operation as demonstrated experimentally in Fig. 21. In fact, no remedial actions or extra hardware is needed for the 3p-DAB to be tolerant to external PL faults.

For other type of faults, such as switch or leg open- and short-circuits, since the 3p-DAB converter is composed of two three-phase inverters, many of the FD strategies and remedial actions proposed for three-phase inverters in the literature [28] are potential candidates for application with the 3p-DAB.

The FD techniques are divided into two groups: component-based and system-based [28]. Component-based techniques are generally integrated within the gate driver circuitry while system-based techniques require external analog circuits or software for analysis of the converter waveforms. The frozen leg operation proposed in [11] and the open-phase operation proposed in this article both rely on component-based FD techniques. However, system-based methods allowing the identification of

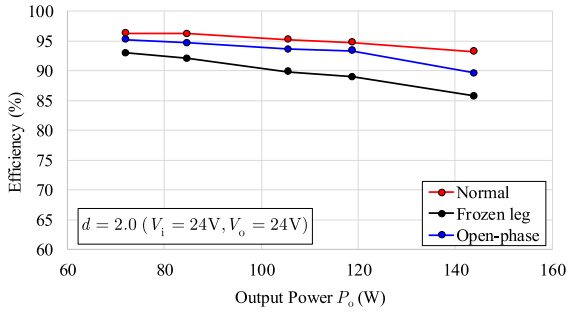

Fig. 22. Efficiency comparison for the experimental prototype.

the faulty phase could also be used. For example, an open-circuit switch fault in inverters leads to a dc component in the faulty-phase currents. This dc component is frequently used for detecting and locating open-circuit switch faults in inverters [29]. This behavior is also present with the 3p-DAB [30]. Other fault cases are open for further research.

Furthermore, as for FD techniques, many remedial actions proposed for inverters such as those investigated in [31]–[34] lead to a post-fault open-phase condition of the inverter. These strategies are generally based on the use of a split bus with triacs and fuses to open the faulty phase. While the cost and efficiency issues of the additional components are important engineering concerns, they are often neglected when fault tolerance and system availability are the main objectives. Nevertheless, it is well known that some of these strategies are not viable in certain applications due to their impacts on efficiency [10].

In this article, the post-fault open-phase FT operation is proposed to be enabled by a feedback fault signal coming from the gate drivers, similarly to the previous article on the frozen leg operation [11]. The demonstrated advantages of the open-phase over frozen leg make interesting the use of the open-phase mode as a first post-fault strategy following the frozen leg condition. This could be the first action before considering oversizing the components or reducing the output power.

Since the 3p-DAB can be operated shortly in frozen leg prior to opening the phase, the opening delay introduced by general-purpose electromechanical relays or contactors is not problematic as shown experimentally in Fig. 20. Moreover, since the 3p-DAB does not exhibit any dc component in the phase current in the frozen leg mode, the phase can be opened using standard ac-rated devices. In the normal operation, the efficiency penalty of adding six (6) switches to open any of the faulty phases is expected to be small if the switches are correctly sized for the phase current. In the case of the prototype presented in this article, the maximum efficiency penalty in the normal operation is 0.5% at $v_i = 24$ V, $v_o = 24$ V, and $P_o = 144$ W. Using NC contacts also avoid increasing the required auxiliary power to keep the relays closed in the normal operation.

Considering the impact of adding the six (6) switches on the overall efficiency, the efficiency of the 3p-DAB prototype is also analyzed in Fig. 22. As expected, due to the increased rms currents, the efficiency is reduced in the frozen leg and open-phase as compared to the normal case. The efficiency in the frozen leg is also reduced as compared to the open-phase case because of the additional reactive current circulating in the faulty phase in the frozen leg operation.

V. Conclusion

In this article, the open-phase FT operation of the 3p-DAB converter is proposed and confirmed experimentally on a closed-loop EPC2022 GaN-based small-scale prototype. The steady-state analysis is performed to evaluate the impact of the open-phase operation on the converter voltage and current waveforms, its power transfer relationship, as well as its soft-switching capabilities. Small-signal analyses along with time-domain simulations are provided to assess the impacts on the converter stability and its transient dynamic performance.

The important conclusions are as follows.

1) The open-phase operation provides reduced current stress and an increased power transfer capability over the frozen leg operation.
2) The power transfer capability in open-phase is theoretically half the one in the normal operation, such that, for the same voltages and loading conditions, the control phase-shift needs to increase.
3) The stability of the 3p-DAB can be positively and/or negatively affected in the open-phase operation.
4) For the same PI controller, the transient response is negatively affected in the open-phase operation such that the controller parameters may need to be adjusted.

Using an FT topology, which provides intrinsic redundancy upon failure of switches, will undeniably facilitate the industrial acceptation of emerging semiconductor technologies such as silicon carbide and GaN.

References

[1] G. S. Thandi, R. Zhang, K. Xing, F. C. Lee, and D. Boroyevich, "Modeling, control and stability analysis of a PEBB based DC DPS," *IEEE Trans. Power Del.*, vol. 14, no. 2, pp. 497–505, Apr. 1999.
[2] M. N. Kheraluwala, R. W. Gascoigne, D. M. Divan, and E. D. Baumann, "Performance characterization of a high-power dual active bridge DC-to-DC converter," *IEEE Trans. Ind. Appl.*, vol. 28, no. 6, pp. 1294–1301, Nov./Dec. 1992.
[3] R. W. A. A. De Doncker, D. M. Divan, and M. H. Kheraluwala, "A three-phase soft-switched high-power-density DC/DC converter for high-power applications," *IEEE Trans. Ind. Appl.*, vol. 27, no. 1, pp. 63–73, Jan./Feb. 1991.
[4] B. Zhao, Q. Song, W. Liu, and Y. Sun, "Overview of dual-active-bridge isolated bidirectional DC–DC converter for high-frequency-link power-conversion system," *IEEE Trans. Power Electron.*, vol. 29, no. 8, pp. 4091–4106, Aug. 2014.
[5] R. W. De Doncker, "Power electronic technologies for flexible DC distribution grids," in *Proc. IEEE Int. Power Electron. Conf.*, May 2014, pp. 736–743.
[6] E. De Din, H. A. B. Siddique, M. Cupelli, A. Monti, and R. W. De Doncker, "Voltage control of parallel-connected dual-active bridge converters for shipboard applications," *IEEE J. Emerg. Sel. Topics Power Electron.*, vol. 6, no. 2, pp. 664–673, Jun. 2018.
[7] N. H. Baars, J. Everts, C. G. E. Wijnands, and E. A. Lomonova, "Performance evaluation of a three-phase dual active bridge DC–DC converter with different transformer winding configurations," *IEEE Trans. Power Electron.*, vol. 31, no. 10, pp. 6814–6823, Oct. 2016.
[8] L. Ferreira Costa and M. Liserre, "Failure analysis of the dc–dc converter: A comprehensive survey of faults and solutions for improving reliability," *IEEE Power Electron. Mag.*, vol. 5, no. 4, pp. 42–51, Dec. 2018.

[9] R. V. White and F. M. Miles, "Principles of fault tolerance," in *Proc. Appl. Power Electron. Conf.*, Mar. 1996, pp. 18–25.
[10] Y. Song and B. Wang, "Survey on reliability of power electronic systems," *IEEE Trans. Power Electron.*, vol. 28, no. 1, pp. 591–604, Jan. 2013.
[11] S. Haghbin, F. Blaabjerg, and A. S. Bahman, "Frozen leg operation of a three-phase dual active bridge converter," *IEEE Trans. Power Electron.*, vol. 34, no. 5, pp. 4239–4248, May 2019.
[12] Z. Yang, J. Hu, G. C. Pasupuleti, and R. W. De Doncker, "Operation-oriented design procedure of a three-phase dual-active bridge converter for a wide operation range," in *Proc. IEEE Energy Convers. Congr. Expo.*, Sep. 2018, pp. 2835–2842.
[13] X. She, A. Q. Huang, and R. Burgos, "Review of solid-state transformer technologies and their application in power distribution systems," *IEEE J. Emerg. Sel. Topics Power Electron.*, vol. 1, no. 3, pp. 186–198, Sep. 2013.
[14] K. Mainali *et al.*, "A transformerless intelligent power substation: A three-phase SST enabled by a 15-kV SiC IGBT," *IEEE Power Electron. Mag.*, vol. 2, no. 3, pp. 31–43, Sep. 2015.
[15] D. Dujic *et al.*, "Power electronic traction transformer-low voltage prototype," *IEEE Trans. Power Electron.*, vol. 28, no. 12, pp. 5522–5534, Dec. 2013.
[16] M. Berger, I. Kocar, H. Fortin-Blanchette, and C. Lavertu, "Hybrid average modeling of three-phase dual active bridge converters for stability analysis," *IEEE Trans. Power Del.*, vol. 33, no. 4, pp. 2020–2029, Aug. 2018.
[17] R. W. Erickson and D. Maksimovic, *Fundamental of Power Electronics*, 2nd ed. Norwell, MA, USA: Kluwer, 2001.
[18] R. D. Middlebrook, "Input filter considerations in design and application of switching regulators," in *Proc. IEEE Ind. Appl. Soc. Conf.*, Oct. 1976, pp. 91–107.
[19] A. Riccobono and E. Santi, "Comprehensive review of stability criteria for DC power distribution systems," *IEEE Trans. Ind. Appl.*, vol. 50, no. 5, pp. 3525–3535, Sep./Oct. 2014.
[20] X. Feng, J. Liu, and F. C. Lee, "Impedance specifications for stable DC distributed power systems," *IEEE Trans. Power Electron.*, vol. 17, no. 2, pp. 157–162, Mar. 2002.
[21] D. Maksimovic, A. M. Stankovic, V. J. Thottuvelil, and G. C. Verghese, "Modeling and simulation of power electronic converters," *Proc. IEEE*, vol. 89, no. 6, pp. 898–912, Jun. 2001.
[22] R. D. Middlebrook and S. Cùk, "A general unified approach to modelling switching-converter power stages," in *Proc. IEEE Power Electron. Spec. Conf.*, Jun. 1976, pp. 18–34.
[23] S. P. Engel, N. Soltau, H. Stagge, and R. W. De Doncker, "Dynamic and balanced control of three-phase high-power dual-active bridge DC–DC converters in DC-grid applications," *IEEE Trans. Power Electron.*, vol. 28, no. 4, pp. 1880–1889, Apr. 2013.
[24] S. R. Sanders, J. M. Noworolski, X. Z. Liu, and G. C. Verghese, "Generalized averaging method for power conversion circuits," *IEEE Trans. Power Electron.*, vol. 6, no. 2, pp. 251–259, Apr. 1991.
[25] H. Qin and J. W. Kimball, "Generalized average modeling of dual active bridge DC-DC converter," *IEEE Trans. Power Electron.*, vol. 27, no. 4, pp. 2078–2084, Apr. 2012.
[26] K. Zhang, Z. Shan, and J. Jatskevich, "Large- and small-signal average value modeling of dual-active-bridge DC-DC converter considering power losses," *IEEE Trans. Power Electron.*, vol. 32, no. 3, pp. 1964–1974, Mar. 2017.
[27] Z. Li, Y. Wang, L. Shi, J. Huang, Y. Cui, and W. Lei, "Generalized averaging modeling and control strategy for three-phase dual-active-bridge DC-DC converters with three control variables," in *Proc. IEEE Appl. Power Electron. Conf. Expo.*, Mar. 2017, pp. 1078–1084.
[28] B. Mirafzal, "Survey of fault-tolerance techniques for three-phase voltage source inverters," *IEEE Trans. Ind. Electron.*, vol. 61, no. 10, pp. 5192–5202, Oct. 2014.
[29] W. Sleszynski, J. Nieznanski, and A. Cichowski, "Open-transistor fault diagnostics in voltage-source inverters by analyzing the load currents," *IEEE Trans. Ind. Electron.*, vol. 56, no. 11, pp. 4681–4688, Nov. 2009.
[30] A. Davoodi, N. Noroozi, and M. R. Zolghadri, "A fault-tolerant strategy for three-phase dual active bridge converter," in *Proc. 10th Int. Power Electron. Drive Syst. Tech. Conf.*, 2019, pp. 253–258.
[31] B. A. Welchko, T. A. Lipo, T. M. Jahns, and S. E. Schulz, "Fault tolerant three-phase AC motor drive topologies: A comparison of features, cost, and limitations," *IEEE Trans. Power Electron .*, vol. 19, no. 4, pp. 1108–1116, Jul. 2004.
[32] R. L. de Araujo Ribeiro, C. B. Jacobina, E. R. C. da Silva, and A. M. N. Lima, "Fault-tolerant voltage-fed PWM inverter AC motor drive systems," *IEEE Trans. Ind. Electron.*, vol. 51, no. 2, pp. 439–446, Apr. 2004.
[33] J.-R. Fu and T. A. Lipo, "A strategy to isolate the switching device fault of a current regulated motor drive," in *Proc. Conf. Rec. IEEE Ind. Appl. Conf. 28th Annu. Meeting*, Toronto, Canada, Oct. 2–8, 1993, pp. 1015–1020.
[34] S. Bolognani, M. Zordan, and M. Zigliotto, "Experimental fault-tolerant control of a PMSM drive," *IEEE Trans. Ind. Electron.*, vol. 47, no. 5, pp. 1134–1141, Oct. 2000.

Maxime Berger (S'14) received the B.Eng. degree in 2016 from the Université du Québec à Rimouski, Rimouski, QC, Canada, in 2014, and the M.A.Sc. degree from Polytechnique Montréal, Montréal, QC, Canada, where he is currently working toward the Ph.D. degree in electrical engineering.

Since 2012, he has been with Bombardier Transportation, St.-Bruno, QC, Canada, where he is working with the Systems Integration Department. His research interests include power electronics, protection, and the simulation and analysis of power systems transients. His research is supported by Bombardier Transportation, the Fonds de Recherche du Québec-Nature et Technologies, and the Natural Sciences and Engineering Research Council of Canada through the Industrial Innovation Scholarship Program.

Ilhan Kocar (M'10–SM'13) received the Ph.D. degree in electrical engineering from École Polytechnique de Montréal affiliated to Université de Montréal, Montréal, QC, Canada, in 2009.

From 1998 to 2004, he was serving as a Project Engineer with Aselsan Electronics Inc., and from 2009 to 2011, he was serving as an R&D Engineer with CYME International T&D. In 2011, he joined the Faculty of Electrical Engineering, Polytechnique Montreal, Montréal, Canada. He works in close collaboration with electric utilities, research organizations, and power system tool developers. His research interests include power system analysis, modeling, and simulation.

Dr. Kocar is a Registered Engineer in the province of Québec.

Handy Fortin-Blanchette (S'07–M'10) received the B.Eng., M.Eng., and Ph.D. degrees in electrical engineering from the École de Technologie Supérieure (ÉTS), Montreal, QC, Canada, in 2001, 2003, and 2010, respectively.

From 1994 to 1997, he was engaged in industrial automation. From 1998 to 2000, he was with the Bombardier Transport-ETS Research Laboratory, Montreal, where he worked on a high power traction system. From 2001 to 2003, he was involved in the development of an electrical drive library for the Simulink (MATLAB) environment. From 2007 to 2010, he was with OPAL-RT Technologies, where he led CPU-based and FPGA-based power electronics real-time simulation projects. From 2010 to 2011, he was a Visiting Scholar with the Center for Power Electronics and System, Virginia Polytechnic Institute and State University, Blacksburg, where he was involved in the packaging of high-temperature converters for aircraft applications. He is currently an Associate Professor of electrical engineering with the École de Technologie Supérieure. His current research interests include EMI prediction, circuit modeling, and high density power converters packaging.

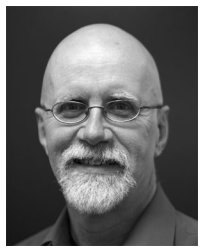

Carl Lavertu (M'17) received the B.Eng. degree in electrical engineering from the Université du Québec à Trois-Rivières, Trois-Rivières, QC, Canada, in 1985.

From 1985 to 1991, he was with Lauzon Lavertu Consultants Inc., Drummondville, QC, Canada. Since 1991, he has been working with Bombardier Transportation, St.-Bruno, QC, Canada, where he is currently a Fellow Expert in Power Electronics. He has been working on various rail projects mainly involved in the design, fabrication, testing of traction and auxiliary power converters, battery systems, door controllers, and lighting systems. He has two U.S. Patents.

Mr. Lavertu is a Registered Professional Engineer in the province of Québec.